

NUMERICAL STUDY OF PITCHING OSCILLATION EFFECT ON AERODYNAMIC CHARACTERISTICS OVER ASYMMETRIC VORTEX STRUCTURE OF SLENDER REVOLUTION

XIA Ming*, LI Dong*, SONG Bi-feng*

***Northwestern polytechnical University, Xi'an 710072, China**

xiaming@comac.cc; ldgh@nwpu.edu.cn; bfsong@nwpu.edu.cn

Keywords: *slender; asymmetrical control; pitching oscillation; detached-Eddy simulation*

Abstract

The unsteady aerodynamic characteristics for a slender revolution under the influence of pitching oscillation at high angle of attack were simulated numerically using DES (Detached-Eddy Simulation) approach.

The numerical results show that the DES model is more suitable for the complex separated flow around the slender body at extremely high angle of attack. Based on DES methods, the location and strength of separated vortex, flow field, pressure distribution on the surface and force coefficients were observed and analyzed. It is found that, the pitching oscillation has strong control ability to the asymmetric separated vortex around slender body, and it would change the construction of flow field, the asymmetrical flow was restrained and tends to symmetrical flow.

1 Introduction

The flow past a slender body of revolution has been investigated using a variety of approaches, these and other investigations have shown that the vortices around slender body of revolution exhibit a wide variety of phenomena as angle of attack increase from zero [1-3]. The steady symmetric vortices are observed in the leeward-side flow at low incidence; with further increase in incidence, the symmetric vortex pair becomes asymmetric, but the flow remains steady in time. At still higher incidence, the steady asymmetric

flow evolves to a pattern of multiple vortices that leave from alternate sides of the body with increasing distance downstream. With further increase in incidence, the separation vortex on the leeside breaks down from the rear slender and the position of vortex breakdown moves upstream, the vortex flow becomes unsteady, and vortex shedding occurs.

Asymmetrical vortex flow over the slender body at high angles of attack will be to induce great side force; it could seriously damage the flexibility and maneuverability of new generation fighter and missiles. For improve the aerodynamic characteristics of slender body at high angle of attack, it is very important to study, forecast and control asymmetric vortices, and it has very powerful practical application value.

To improve the flexibility and agility of aircraft, the control methods of vortex structures are so widely used and respected. It was found in practice that the strong coupling effects exist between the asymmetric flow separation and nonsteady motion of slender body. The prediction of this coupling has a great influence in improving aerodynamic characteristics of the aircraft in high angle of attack. For the past few years, by imposing nonsteady motion on the slender, researchers could control asymmetric flow field on the leeside of the slender. Coupled effect between unsymmetrical separation on the backside and slender nonsteady motion was investigated using numerical simulation method [4-6].

Numerical models of the flow around slender body of revolution are challenged by the asymmetrical features at high angle of attack. For the massive asymmetric separation of slender body at high angle of attack, the RANS models often fail to capture the effects of strong pressure gradients with separated flow, and the application of large-eddy simulation (LES) [7] is limited by the high computational costs at high Reynolds number, especially for configurations with boundary layers. To overcome the deficiencies of RANS and LES, the hybrid RANS/LES turbulence method (DES), applies the Spalart-Allmaras model in the RANS boundary layer region, and LES to the majority of the flow domain, the approach is approved to be a good way of taking advantage of the merits of both RANS and LES. It was demonstrated the DES model could compute number of complex flow structure problems around aircraft successfully, including delta wing vortex breakdown [8] and the F/A-18E with unsteady shock buffet [9], etc.

In the following segment, DES will be used as the foundation of study in the pitching oscillation simulation over slender revolution. The primary interest in the studies of pitching oscillation included main vertical structure on the leeward and integral parameters such as side-force coefficient and distribution of the mean pressure around the section. It is found that, the pitching oscillation at fixed frequency has strong control ability to the slender body at high angles of attack, and it would change the construction of flow field, the asymmetrical flow was restrained and tends to symmetrical flow.

2 Computational Methods

2.1 Governing Equations

In the present study, the turbulent flow around a circular cylinder is computed with the three-dimensional compressible Navier-Stokes (N-S) Equations, the equations of mass, momentum, and energy can be written in integral form as,

$$\iiint_{\Omega} \frac{\partial \mathbf{W}}{\partial t} dV + \iint_{\partial\Omega} \overline{\mathbf{H}} \cdot \mathbf{n} dS = \iint_{\partial\Omega} \overline{\mathbf{H}}_v \cdot \mathbf{n} dS \quad (1)$$

where,

$$\mathbf{W} = \begin{bmatrix} \rho \\ \rho u \\ \rho v \\ \rho w \\ \rho E \end{bmatrix} \quad (2)$$

$$\overline{\mathbf{H}} = \begin{bmatrix} \rho \mathbf{q} \\ \rho u \mathbf{q} + p \mathbf{I}_x \\ \rho v \mathbf{q} + p \mathbf{I}_y \\ \rho w \mathbf{q} + p \mathbf{I}_z \\ \rho H \mathbf{q} \end{bmatrix} \quad (3)$$

$$\overline{\mathbf{H}}_v = \begin{bmatrix} 0 \\ \tau_{xx} \mathbf{I}_x + \tau_{xy} \mathbf{I}_y + \tau_{xz} \mathbf{I}_z \\ \tau_{xy} \mathbf{I}_x + \tau_{yy} \mathbf{I}_y + \tau_{yz} \mathbf{I}_z \\ \tau_{xz} \mathbf{I}_x + \tau_{yz} \mathbf{I}_y + \tau_{zz} \mathbf{I}_z \\ \beta_x \mathbf{I}_x + \beta_y \mathbf{I}_y + \beta_z \mathbf{I}_z \end{bmatrix} \quad (4)$$

A fluid element volume over which the equations are enforced is denoted by Ω (the boundary surface is denoted with outward pointing unit normal). The Cartesian unit vectors are \mathbf{I}_x , \mathbf{I}_y and \mathbf{I}_z .

ρ is the density, p is the pressure, and \mathbf{q} is the velocity vector.

$$\mathbf{q} = (u, v, w)^T \quad (5)$$

τ are the viscous stress tensor components. Closure of this system of equations is provided by the perfect gas law and two equations of state are needed,

$$P = \rho(\gamma - 1)[E - 0.5(u^2 + v^2 + w^2)] \quad (6)$$

$$T = p / (R\rho) \quad (7)$$

2.2 S-A Model

The S-A one equation model computes the eddy viscosity by the use of a single transport equation. The model possesses satisfactory numerical characteristics in terms of near-wall resolution. The model solves a single partial differential equation for a working $\tilde{\nu}$ and is written as,

$$\begin{aligned} \frac{D\tilde{\nu}}{Dt} &= c_{bl}(1 - f_{t2})\tilde{\nu} - \\ &(c_{w1}f_w - \frac{c_{bl}}{k^2}f_{t2})[\frac{\tilde{\nu}}{d}]^2 + \\ &\frac{1}{\sigma}[\nabla \cdot ((v + \tilde{\nu})\nabla\tilde{\nu}) + c_{b2}(\nabla\tilde{\nu})^2] \end{aligned} \quad (8)$$

Where the eddy viscosity ν_t is obtained from

$$\nu_t = \tilde{\nu}f_{v1} \quad (9)$$

$$f_{v1} = \frac{\chi^3}{\chi^3 + c_{v1}^3} \quad (10)$$

$$\chi = \frac{\tilde{\nu}}{\nu} \quad (11)$$

$$\chi = \frac{\tilde{\nu}}{\nu} \quad (12)$$

$$\tilde{S} = S + \frac{\tilde{\nu}}{k^2d^2}f_{v2} \quad (13)$$

$$f_{v2} = 1 - \frac{\chi}{1 + \chi f_{v1}} \quad (14)$$

And S is the magnitude of the vorticity given by

$$S = |w| = \left| \nabla \times (u\hat{i} + v\hat{j} + w\hat{k}) \right| \quad (15)$$

where d is the distance to the slender wall.

2.3 DES

The Detached Eddy Simulation (DES) model [10] is built upon the one-equation S-A RANS model. To obtain the DES-SA formulation, the distance to the wall d in the S-A model is replaced by a length scale that is the lesser of d and a length proportional to the local grid spacing Δ . The constant C_{DES} is set to 0.65 consistent with the structured grid implementation, and Δ is taken to be the longest distance between the ell center and all of the neighboring cell centers. When $d < C_{DES}\Delta$, the hybrid model acts as the RANS in the detached flow region and when $d > C_{DES}\Delta$, the model acts as the LES in the separated flow region.

$$\tilde{d} \equiv \min(d, C_{DES}\Delta) \quad (16)$$

$$\Delta = \max(\Delta x, \Delta y, \Delta z) \quad (17)$$

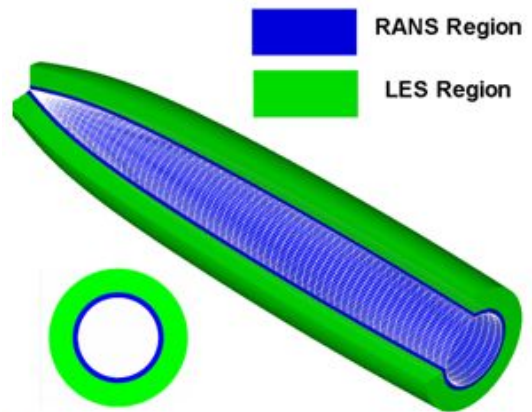


Figure1 Division of flow-field for DES

Figure 1 display the division of flow-field for DES around slender body, the flow field was separated into two parts by length scales, which are called the RANS region and the LES region, respectively.

2.4 Body configurations and Computational Grids

All models calculated were a 2.0-diam tangent ogive forebody with a 5.5 diameters cylinder afterbody extending aft of the slender body to $x/D = 7.5$, and D is the nondimensional cylinder diameter, which typically have regions of separated flow, and the experimental data were provided by Lamont [11].

The present calculations are performed on H-O type computational grids shown in Fig 2. The grid with 3.5 million cells has been used with 201 cells in the axial direction, 141 in radial direction and 121 in circumferential, the spacing is stretched in the radial direction and the initial near-slender surface spacing is $1 \times 10^{-5} D$.

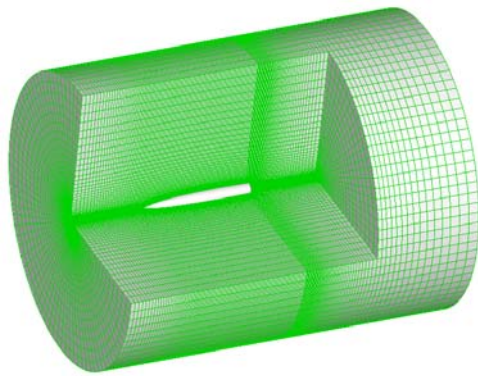


Figure2 Computational Grid

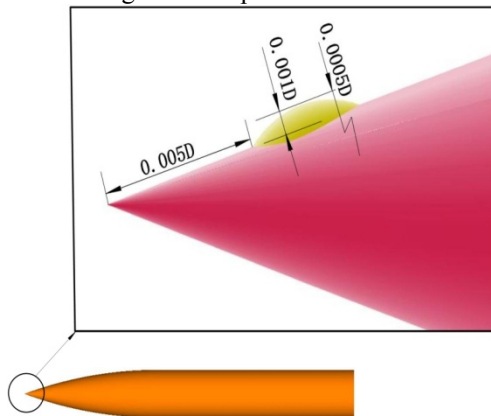


Figure3. Model of manual disturbance

It has been proved by the numerical simulation [12] that the experimentally observed asymmetric flow is numerically simulated by the introduction of a simulated disturbance placed near the body apex. In the present study, we set up a spherical disturbance on the tip of slender body, the height of the bump is $h=0.001D$, the graph of disturbance is shown in Figure 3.

The initial conditions are set as the free-stream variables. No-slip and adiabatic condition applied at the slender body wall. Undisturbed freestream conditions are maintained at the computational outer boundary, and all the used grids extended to 11 body diameters in the radial direction, the computed body length was extended 5.0 diameters in front and 10.0 diameters in rear beyond the physical body length to minimize the effect of the outflow.

3 Results and Discussion

3.1 Pitching Oscillation from $\alpha_0=55^\circ$

In the present calculation, the freestream Mach number was 0.28, and $Re_D = 3.0 \times 10^6$ with angle of attack $\alpha = 55^\circ$. Under the current condition, the flow patterns in the leeside of slender was multi-asymmetric vortices system flow [11], but the axial flow along slender was still strong, and it is enough to remain steady for flowfield and separated vortex.

Apply a pitching oscillation to slender body, the starting angle of attack is $\alpha_0=55^\circ$, the instantaneous angle of attack :

$$\alpha = \alpha_0 + A \cdot \sin(\omega \cdot t) \quad (18)$$

where $A = 3^\circ$, $\omega = 1$.

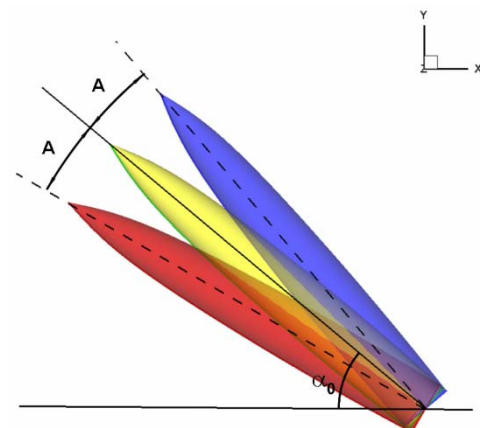


Figure4 Oscillation maneuver of slender body

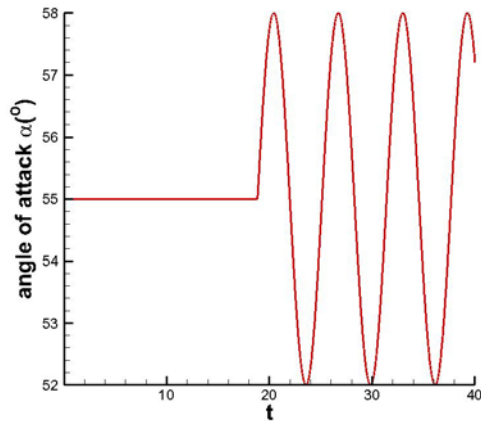


Figure5 Time history of instant angle of attack from $\alpha_0=55^\circ$

Figure 4 is the description of slender pitching and the time history of instantaneous angle of attack is shown in Figure 5. In order to observe the effect of pitching oscillation on the characteristics of asymmetric vortex better, the pitching oscillation was induced from $t=18.84$.

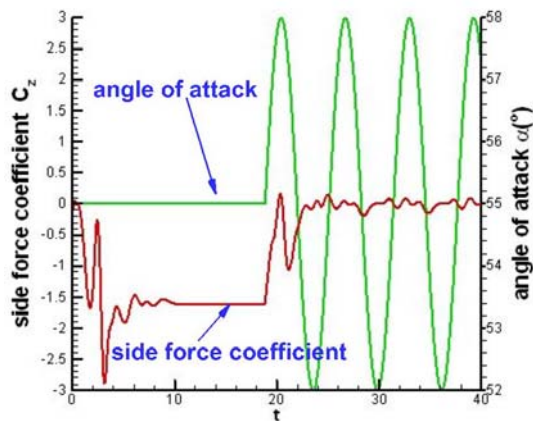


Figure6. Side Force coefficient history with nondimensional time:

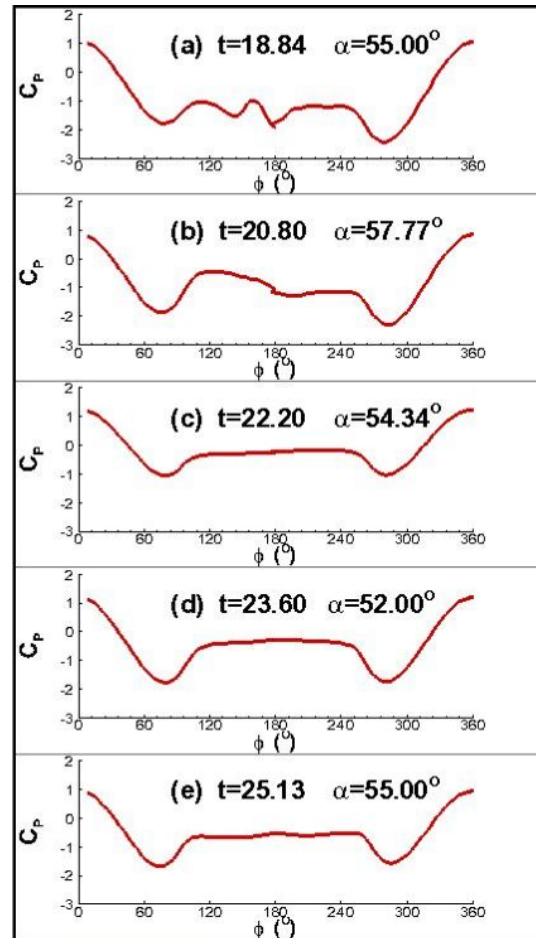


Figure7. Pressure coefficient distribution at $x/d=4.0$ in the first vibration cycle

Time-history of the side force coefficient following the introduction of disturbance is shown in Figure 6, and the left y-axis is the amplitude of side force coefficient, the right y-axis is the instantaneous angle of attack, the pitching oscillation started from $t=18.81$. The pitching oscillation cause the side force tends to decay quickly and relatively toward a small value, with only small-scale fluctuations. The mean value of the side-force coefficient tends toward to 0, which means the asymmetric character of separated flow has come under the suppression a very great degree.

Fig.7 shows the variance of pressure coefficient distribution at $x/d=4.0$ in the first pitching oscillation cycle, it is seen that the pressure coefficient distribution grew more and more symmetrical on each side of section, and the pressure distribution was under the state of symmetric even slender body have not finished the first oscillation cycle.

3.2 Pitching Oscillation from $\alpha_0=70^\circ$

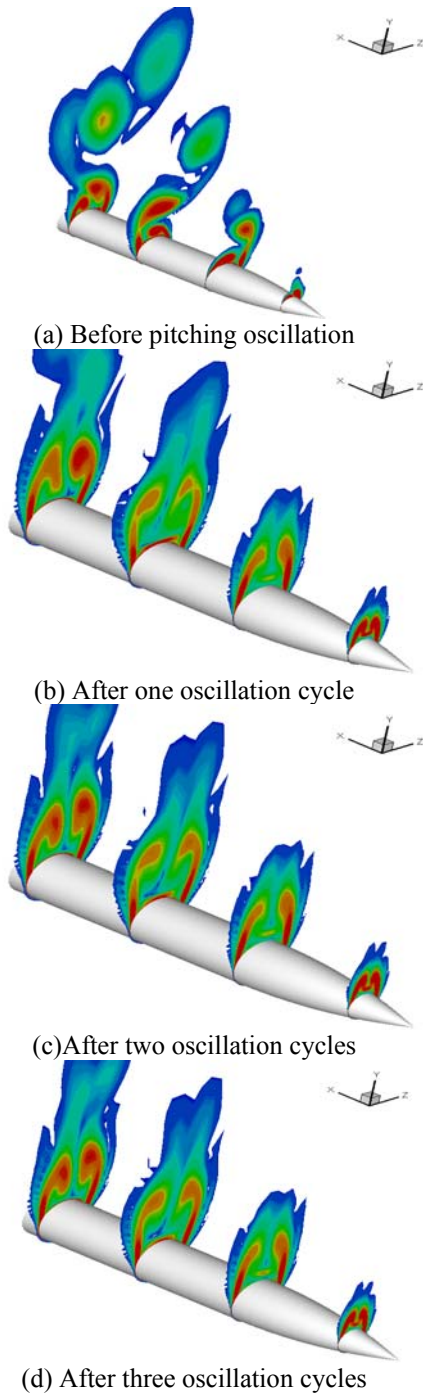


Figure8 Flowfield around the circular cylinder during pitching oscillation ($\alpha_0=55^\circ$)

As can be seen from fig. 8, the pitching oscillation at current pitching amplitude and frequency could change the construction of flow field. The asymmetrical separated vortex was restrained and translated to symmetric flow just after one pitching oscillation. Furthermore, it is found from Figure 8(c) and (d), the symmetry will to be to maintain if such oscillation continues.

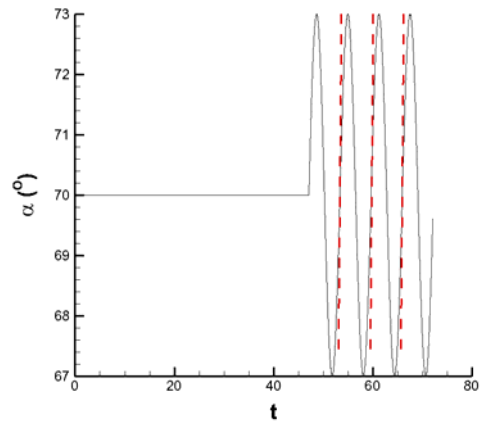


Figure9 Time history of instant angle of attack from $\alpha_0=70^\circ$

Figure 9 shows the incidence history in present section, the unsteady flows around slender body undergoing time-dependent maneuver. Starting with a stability and periodic solution from time $t=47.10$ and angle of attack $\alpha_0=70^\circ$.

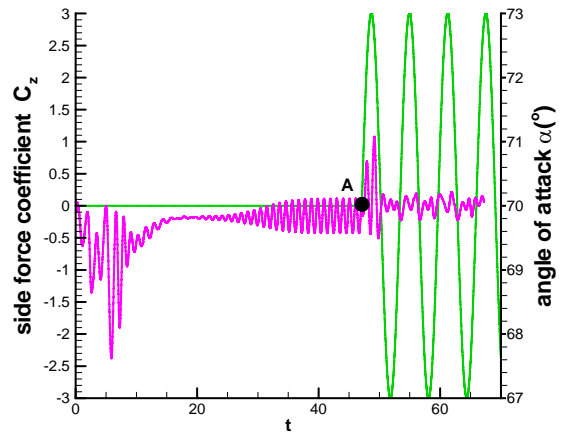


Fig.10 History of body side force coefficient in oscillation

Figure 10 show the history of the instantaneous side force in different cycle during pitching oscillation. After inducing pitching oscillation from point A, the force coefficient became much closer to zero. From the variation of average side force, it is clear that the value of side force decreases quickly during pitching, and decline most rapidly in the first oscillation cycle. The value of side force dropped swiftly towards zero, and in a constant state of very small magnitude.

Numerical study of pitching oscillation effect on aerodynamic characteristics over Asymmetric vortex structure of slender revolution

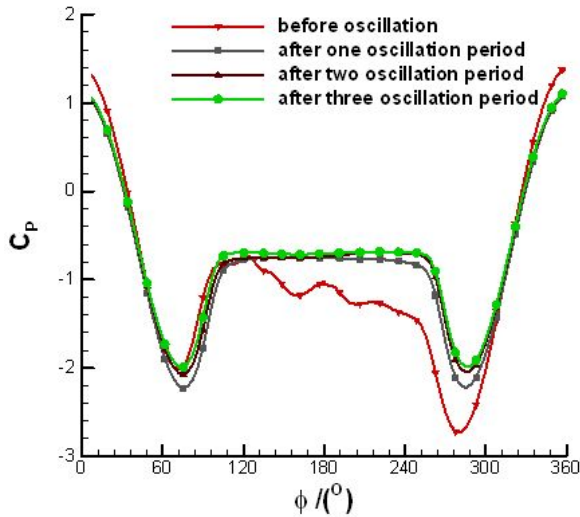
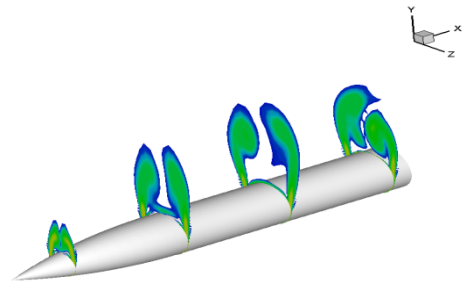
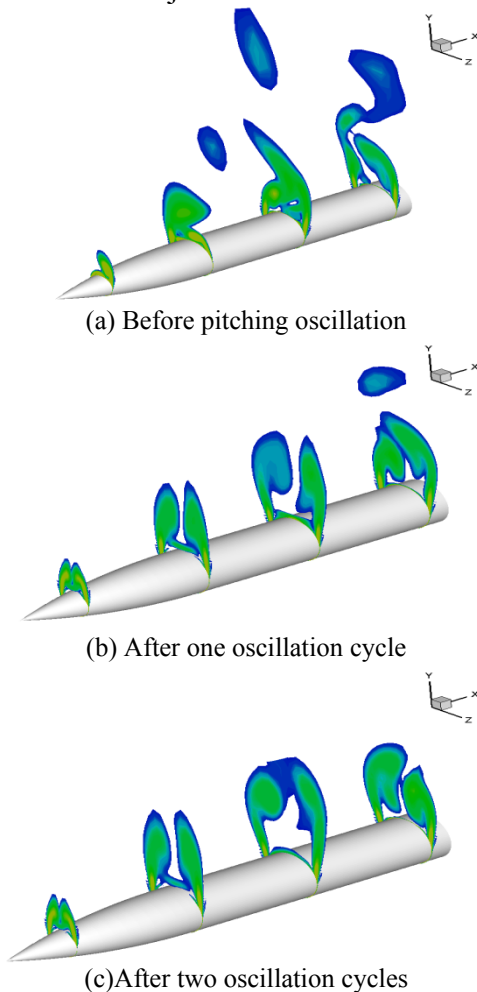


Fig.11 Pressure coefficient distribution at $x/D=5.0$ in the pitching oscillation

Corresponding pressure coefficient distribution with different pitching period is shown in Figure 11, from which can be seen the pitching oscillation constrains the asymmetry and converted the pressure distribution to symmetrical state just after one oscillation cycle.



(d) After three oscillation cycles

Figure12 Flowfield around the circular cylinder during pitching oscillation ($\alpha_0=70^\circ$)

Figure 12 shows the vorticity flow field in the leeside of slender revolution at the beginning of pitching, after one oscillation cycle, after two cycles and after three cycles. It is clear that just after one pitching oscillation cycle, the asymmetric flowfield developed to a symmetry, and the symmetrical state can maintained as long as the slender revolution under pitching oscillation.

4 Conclusions

DES model based on S-A is presented here to simulate the aerodynamics characteristics under the influence of pitching oscillation at two typical starting angles of attack with different frequencies and amplitudes. In multi-asymmetric vortices system flow at high angle of attack and multi-asymmetric vortices break down at extremely high angle of attack, the pitching oscillation has strong control ability, the side force decreased significantly under pitching; the asymmetrical flow was restrained and tends to symmetrical flow.

References

- [1] HUNT, B.L. Asymmetric Vortex Wakes on Slender Bodies. AIAA Paper 82-1336, AIAA 9th Atmospheric Flight Mechanic Meeting, August 1982.
- [2] Degani, D. and Zilliac, G.G. Experimental Study of the Flow around an Ogive-Cylinder at Incidence. AIAA Paper 88-4330, AIAA 15th Atmospheric Flight Mechanics Conference, August 1988.
- [3] Degani, D. and Zilliac, G.G. An Experimental Study of the Nonsteady Asymmetric Flow around an Ogive-cylinder at high Incidence. AIAA Journal, 1989.
- [4] M.J. Stanek and M.R. Visbal. Investigation of vortex development in a pitching slender body of revolution. Journal of Aircraft, 30(5):711-718, 1993.

- [5] Hoang, N.T., Wetzel, T.G., and Simpson, R.L., unsteady measurement over a 6:1 prolate spheroid undergoing a pitch-up maneuver, AIAA Paper 94-0197, 1994.
- [6] Hoang, N.T., Wetzel, T.G., and Simpson, R.L., Surface pressure measurements over a 6:1 prolate spheroid undergoing time-development maneuver, AIAA Paper 94-1908-CP, 1994.
- [7] Charles GS. Turbulence modeling for time-dependent RANS and VLES: a review. AIAA Paper 97-2051, 1997.
- [8] Scott A. Morton, James R. Forsythe, Anthony M. Mitchell, and David Hajek, DES and RANS Simulations of Delta Wing Vortical Flows, AIAA Paper 2002-0587, Jan. 2002.
- [9] Scott A. Morton, Matthew B. Steenman, Russell M. Cummings, and James R. Forsythe, DES Grid Resolution Issues for Vortical Flows on a Delta Wing and an F-18C, AIAA Paper 2003-1103, Jan. 2003.
- [10] Spart PR, Jou W-H, Strelets M, Allmaras SR. Comments on the feasibility of LES for wings, and on a hybrid RANS/LES approach. First AFOESR International Conference on DNS/LES. Ruston, LA; In Advances in DES/LES, Liu C, Liu Z(eds). Greyden Press: Columbus, OH, 1997.
- [11] Lamont PJ. Pressure Measurements on an Ogive-Cylinder at High Angles of Attack with Laminar, Transitional, or Turbulent Separation. AIAA Paper 80-1556, 1980.
- [12] Yuval Levy, Lambertus Hesselink, David Degani. Systematic study of the correlation between geometrical disturbances and flow asymmetries. AIAA Journal, 34(4):772-777, 1996.

Copyright Statement

The authors confirm that they, and/or their company or organization, hold copyright on all of the original material included in this paper. The authors also confirm that they have obtained permission, from the copyright holder of any third party material included in this paper, to publish it as part of their paper. The authors confirm that they give permission, or have obtained permission from the copyright holder of this paper, for the publication and distribution of this paper as part of the ICAS2012 proceedings or as individual off-prints from the proceedings.